Environmental Science & Technology

pubs.acs.org/est

Article

New Route to Toxic Nitro and Nitroso Products upon Irradiation of Micropollutant Mixtures Containing Imidacloprid: Role of NO_x and Effect of Natural Organic Matter

Davide Palma, Yara Arbid, Mohamad Sleiman,* Pascal de Sainte-Claire, and Claire Richard*

Cite This: *Environ. Sci. Technol.* 2020, 54, 3325−3333

Read Online

ACCESS | Metrics & More | Article Recommendations | Supporting Information

ABSTRACT: In this study, we reveal the capacity of imidacloprid (a neonicotinoid insecticide) to photoinduce the nitration and nitrosation of three aromatic probes (phenol, resorcinol, and tryptophan) in water. Using a gas-flow reactor and a NO_x analyzer, the production of gaseous NO/NO_2 was demonstrated during irradiation (300−450 nm) of imidacloprid (10^{-4} M). Quantum calculations showed that the formation of NO_x proceeds via homolytic cleavage of the $RN-NO_2$ bond in the triplet state. In addition to gaseous NO/NO_2, nitrite and nitrate were also detected in water, with the following mass balance: 40 ± 8% for NO_2, 2 ± 0.5% for NO, 52 ± 5% for NO_3^-, and 16 ± 2% for NO_2^-. The formation of nitro/nitroso probe derivatives was evidenced by high-resolution mass spectrometry, and their yields were found to range between 0.08 and 5.1%. The contribution of NO_3^-/NO_2^- to the nitration and nitrosation processes was found to be minor under our experimental conditions. In contrast, the addition of natural organic matter (NOM) significantly enhanced the yields of nitro/nitroso derivatives, likely via the production of triplet excited states (^{3}NOM*) and $HO^\bullet$. These findings reveal the importance of investigating the photochemical reactivity of water contaminants in a mixture to better understand the cocktail effects on their fate and toxicity.

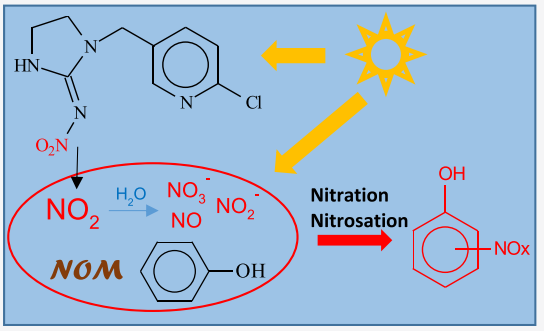

INTRODUCTION

Imidacloprid (1-[(6-chloropyridin-3-yl)methyl]-*N*-nitro-imidazolidin-2-imine, IMD, Scheme 1) is a widely used and effective neonicotinoid insecticide.[1] IMD, like other neonicotenoids, is used in a variety of crops, and its applications have been recently extended to the domestic sector and animal health.[1] Once released into the environment, it can reach the aquatic, atmospheric, and terrestrial compartments and be in contact with a lot of living organisms.[2−4] IMD affects the central nervous system of insects,[5] and there are increasing concerns about its deleterious effects with confirmed toxicity for pollinators, especially bees.[6] Toxicity or adverse effects in other species have also been reported.[7−9]

Scheme 1. Molecular Structure of IMD and Its Main Photoproducts

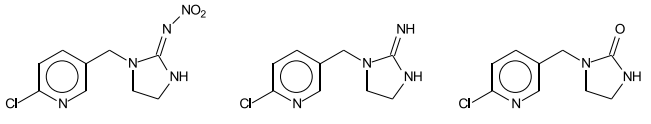

Several studies have been performed to investigate the fate of IMD under solar light, mainly in aqueous solutions,[1,10−13] on plant leaves and cuticles,[14−16] and more recently on solid thin films.[17] Desnitro-IMD (1-[(6-chloropyridin-3-yl)methyl]-imidazolidin-2-imine) was reported to be the main photoproduct and the urea-IMD (1-[(6-chloropyridin-3-yl)methyl]-imidazolidin-2-one) is a minor photoproduct (Scheme 1).[16] The formation of these byproducts seems to imply the cleavage of the $N-NO_2$ bond; however, the fate of NO_2 is not yet clear. Recently, the formation of gaseous nitrogen oxides during the irradiation of IMD at the surface of a germanium attenuated total reflectance crystal was investigated.[17] The authors detected nitrous oxide (N_2O), which was proposed to be formed by the recombination of detached NO_2 with the IMD fragments, in the electronic ground state.

In previous studies, we showed that the fungicides chlorothalonil and thiophanate-methyl can photoinduce the degradation of other pesticides during irradiation.[18,19] These reactions can take place in surface waters, where fungicides are present together with a wide range of other chemicals, and on solid supports such as the surface of leaves, where pesticides are often applied in combination. However, the effect that a

Received: December 11, 2019
Revised: February 10, 2020
Accepted: February 15, 2020
Published: February 15, 2020

pollutant can have on another pollutant remains largely overlooked in photochemical studies, and little is known about the transformation of photostable pollutants via light-induced reactive intermediates of other co-pollutants. The ability of IMD to release NO_2 upon irradiation makes this compound important to study in this context because nitration of chemicals has been reported in a lot of systems generating NO_2.[20−28]

The goal of this study was thus to explore the formation of reactive NO_x via IMD photolysis and their reactivity toward surrogates of water contaminants and typical moieties of natural organic matter (NOM; phenol, resorcinol, and tryptophan). In particular, we investigated the formation of nitro- and nitroso-derivatives, two potentially toxic categories of compounds, from the three selected probes under polychromatic irradiation (300−450 nm) in the presence of IMD. Experiments were carried out using a flow-tube reactor equipped with a NO_x analyzer, whereas the formation of byproducts was characterized by high-resolution ultrahigh-performance liquid chromatography system−electrospray ionization-mass spectrometry (UHPLC−ESI-MS). Theoretical calculations were also performed to elucidate the mechanisms of NO_x formation. To the best of our knowledge, this is the first study reporting on the measurement of NO_x during irradiation of IMD in water and on their role in nitrosation/nitration of other water pollutants. Environmental implications of this light-induced indirect degradation are discussed.

MATERIALS AND METHODS

Chemicals and Materials. Imidacloprid (PESTANAL, analytical standard), resorcinol (purity 99%), phenol (purity ≥ 99.5%), L-tryptophan (purity ≥ 98%), and 2,4-dinitrophenylhydrazine (DNPH, purity 97%) were purchased from Sigma-Aldrich and used as received. Sodium nitrite (Rectapur 98%), sodium nitrate (Fluka, purity 99%), 2- and 4-nitrophenol (Fluka, purity ≥ 99%), and 4-nitrosophenol (Aldrich-Chemie, purity 60% due to the water content of 40%) were also used without further purification. Suwannee River NOM (2R101N) was purchased from IHSS. Water was purified using a reverse osmosis RiOs 5 and Synergy (Millipore) device (resistivity 18 MΩ cm, DOC < 0.1 mg·L^{-1}). All solvents or other reactants were of the highest grade available.

Irradiation. Two different irradiation devices were used. To monitor NO_x formation in the gas phase, device 1 was designed with a cylindrical Pyrex gas flow reactor (0.65 L, length 27 cm, and diameter 5.7 cm) containing 200 mL of IMD solution (10^{-4} M or 25.6 mg·L^{-1}) and irradiated from the top with two fluorescent tubes (Sylvania F15W/BL 368, 438 mm × 26 mm, 300−450 nm, and λ_{max} at 365 nm, see Figure S1) placed at a distance of 5 cm. The rate of incident light entering the solution was measured using a QE65000 radiometer (Ocean Optics); it was equal to 1.3×10^{16} photon·cm^{-2}·s^{-1}. The gas flow reactor was connected to a NO_x chemiluminescence analyzer (Thermo Scientific i-42 NO_x analyzer), as shown in Figure 1. Experiments were carried out under a continuous flow of clean air to reduce the residence time of NO_x and minimize NO_2 photolysis. The gaseous inlet of the reactor was connected to flow controllers for N_2 and O_2 (model Brooks 4800 Series), allowing the selection of the atmosphere under which irradiation was performed (pure N_2, pure O_2, or a 80/20 O_2/N_2 mixture) and to adjust the flow rate to 0.7 L min^{-1}. Background levels of NO_x in the gas inlet were negligible (<0.4 ppbv). Before irradiation, the levels of NO_x in the gas phase of the reactor were monitored continuously every 10 s until they reached a steady state within a few minutes (Figure S2). Despite the fact that NO_2 concentrations of up to 40 ppbv were detected initially (first 30 s), a background level of NO_x (<5 ppbv) was quickly reached. This production of NO_2 might possibly be due to IMD photolysis under indoor lighting during the preparation and handling of the solutions. During IMD irradiation, we have chosen to monitor NO_x levels in the gas phase of the reactor at selected times and not continuously. After selected irradiation times, the light was turned off, and the outlet of the reactor was connected to the NO_x analyzer. NO_x levels were measured every 10 s for a period of 1−2 min at a flow rate of 0.7 L min^{-1}. The time profile of NO_x concentrations shown in Figure S2 corresponds to the decay of the NO_x level in the reactor due to dilution with clean air. The level of NO_x measured was relatively constant at 1, 2, 4, and 6 h of IMD irradiation, in accordance with a steady-state regime. The levels of NO_x generated were then obtained by integrating the time profiles of NO_x concentrations. For calculating the yields of NO_x, the ratio of NO_x concentrations (ppbv) was converted into molar by taking into account the gas phase volume of the reactor (450 mL). By measuring the converted quantity (in moles) of IMD during the irradiation period, it was possible to calculate the molar yield for NO and NO_2.

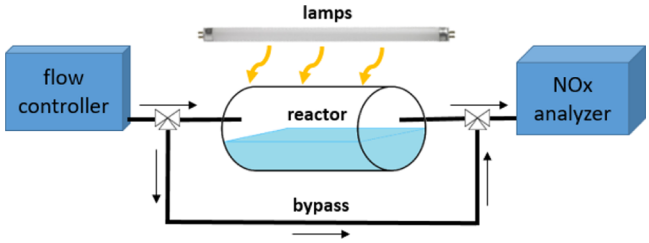

Figure 1. Schematic representation of device 1 used to monitor NO_x formation upon irradiation of IMD solutions.

A second device, device 2, was used to monitor the formation of nitro- and nitroso-derivatives. Fifteen milliliters of solutions was placed in a cylindrical Pyrex reactor sealed with an air-tight silicon cap and surrounded by six fluorescent tubes (Sylvania F15W/BL 368), installed inside a custom-made cylindrical irradiation device. Solutions were not buffered, but pH was controlled during the reactions. The initial pH was 6.5 ± 0.3, and in the course of the reactions, the pH was set to above 5. In the case of IMD + resorcinol mixtures, aliquots were sampled after several selected irradiation times, and the consumption profiles of IMD and nitro- and nitroso-resorcinol were obtained. For IMD + phenol and IMD + tryptophan mixtures and experiments with nitrate/nitrite and NOM, aliquots were only sampled after 16 h of irradiation. Samples were analyzed by HPLC to monitor the loss of IMD and the probes and by UHPLC−high-resolution mass spectrometry (HRMS) to characterize the photoproducts and estimate their levels. For the experiment with 10^{-5} M IMD and 10^{-4} M resorcinol, 75 mL was irradiated in portions of 25 mL, and water was evaporated up to 6 mL using a rotavapor before further analyses. Experiments were done in duplicate or triplicate.

Analytical methods. Absorption spectra were recorded using a Varian Cary 3 spectrophotometer. IMD, phenol, resorcinol, and L-tryptophan concentrations were monitored by HPLC (Waters Alliance 2695) equipped with a photodiode

https://dx.doi.org/10.1021/acs.est.9b07304
Environ. Sci. Technol. 2020, 54, 3325−3333

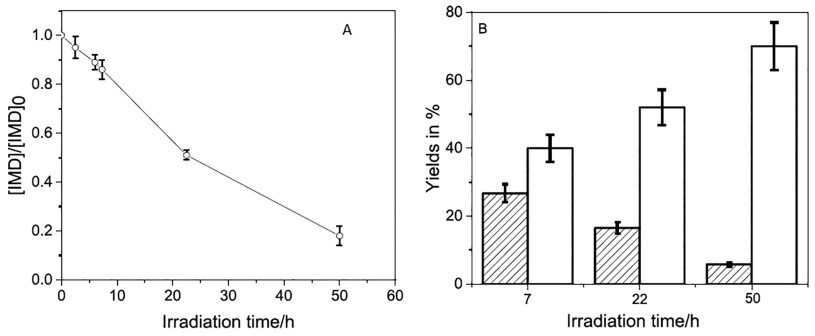

Figure 2. Consumption profile of aqueous IMD (10^{-4} M) irradiated in device 1 (A) and yields of NO_3^- (white bars) and NO_2^- (shaded bars) (B). Error bars are standard deviations.

array detector (Waters 2996) and an EC150/4.6 Nucleodur 100-5 C_8 endcapped column. The HPLC conditions are presented in Table S1. Photoproducts were quantified using the same instrument after derivatization with DNPH.[29] The derivatizing solution (15 mL) was prepared by mixing concentrated HCl, ultrapure water, and acetonitrile at a ratio of 2:5:1. Fifty microliters of this solution was added to 5 mL of sample solution. The derivatization reaction was completed in 5 min, and HPLC analyses were run shortly after. Calibration used derivatized NO_2^- solutions in the concentration range 10^{-6} to 10^{-5} M. All the HPLC analyses were done in triplicate, and the presented data are the mean values obtained.

NO_3^- was measured by ionic chromatography on a Dionex ICS-5000$^+$ using a column model Dionex Ion Pack AS11 2 mm × 250 mm; the flow was 0.25 mL·min^{-1}; and the mobile phase was an aqueous solution of KOH at the concentration of 0.43 mM for the first 4.5 min followed by linear gradient for up to 18 min of runtime by increasing the KOH concentration up to 11.70 mM. The injection volume was 750 μL, and the temperature of the column oven was set to 30 °C. External standards were prepared using $NaNO_3$ in the concentration range 50−200 μg·L^{-1}. Nitro- and nitroso-derivatives of phenol, resorcinol, and L-tryptophan were characterized, and their concentrations were estimated by HRMS performed on an Orbitrap Q-Exactive (Thermo Scientific) coupled to an UHPLC system, Ultimate 3000 RSLC (Thermo Scientific). Because of the lack of available standards, desnitro-IMD and the minor photoproducts were tentatively identified by HRMS, but quantification was not possible. Analyses were carried out in both negative (ESI$^-$) and positive (ESI$^+$) electrospray modes. The column used was the same column used for HPLC-UV. The binary solvent system was composed of acetonitrile and acidified water using formic acid at 40 and 60%, respectively, with a flow rate of 1.0 mL min^{-1}. Nitro- and nitroso-phenols were quantified by the injection of external standards of 4-nitro and 4-nitroso-phenols at concentrations varying from 5×10^{-7} to 4×10^{-6} M (Figure S3). Because of commercial unavailability of nitrated derivatives, the concentrations of nitro- and nitroso-resorcinols were estimated using the calibration curves of 4-nitro- and 4-nitroso-phenols. The concentrations of nitro-tryptophan and nitroso-tryptophan were estimated using L-tryptophan at the concentration of 10^{-6} M as a reference. Yields were obtained by dividing the photoproducts' concentrations by the loss of IMD in concentration and by multiplying these ratios by 100.

Computational Method. Potential energy surfaces (PESs) were investigated with the Gaussian series of programs.[30] Density functional theory (DFT) calculations (optimizations, frequency calculations, identification of transition states, and IRC calculations) were performed at the MN12SX/6-311++G(d,p)//MN12SX/6-31+G(d,p) level of calculation. Among the large set of hybrid range-separated functionals that we tested, MN12SX[31] gave the best agreement between the experimental and theoretical absorption spectra. Finally, the time-dependent-DFT (TD-DFT) method was used to compute singlet excited states. The triplet state was explored with conventional self-consistent field calculations. The solvent was modeled implicitly with the polarizable continuum model (PCM). Electronic energies are reported throughout (Gibbs free energies are not provided here because low vibrational modes may introduce large uncertainties in this calculation).

RESULTS AND DISCUSSION

Photolysis of IMD. The degradation profile of neutral aqueous IMD (10^{-4} M) irradiated in device 1 is shown in Figure 2A. HPLC-UV and UHPLC−HRMS analyses indicated that the main photoproduct was desnitro-IMD (Figure S4). Three minor photoproducts were also found: a compound produced by addition of an oxygen atom on IMD (IMD + O), another one produced by addition of two oxygen atoms on desnitro-IMD (desnitro-IMD + 2O), and the nitroso derivative of IMD (IMD-O) as traces (Table S2).

NO_3^- and NO_2^- were detected in the aqueous phase (Figure S4). The yield of NO_3^- increased constantly to reach 72 ± 5% after 50 h of irradiation (Figure 2B, white bars). In contrast, the yield of NO_2^- decreased from 27% after 7 h of irradiation to 6% after 50 h (Figure 2B, shaded bars). The higher accumulation of NO_3^- compared to that of NO_2^- is consistent with the spectral properties and the known photoreactivity of these ions. NO_3^- (λ_{max} = 300 nm and ε = 8 M^{-1}·cm^{-1}) absorbs much less solar light than NO_2^- (λ_{max} = 355 nm and ε = 22 M^{-1}·cm^{-1}), and its quantum yield of photolysis is also lower (reactions 1−4) leading to a smaller photolysis rate[32]

$$NO_3^- + h\nu \rightarrow NO_2 + O^{\bullet -} \qquad \Phi \approx 0.01 \tag{1}$$

$$NO_3^- + h\nu \rightarrow NO_2^- + O(^3P) \qquad \Phi \approx 0.001 \tag{2}$$

$$NO_2^- + h\nu + H^+ \rightarrow NO + HO^{\bullet} \qquad \Phi = 0.025 \tag{3}$$

$$NO_2^- + h\nu \rightarrow NO_2 + e_{aq}^- \qquad \Phi < 0.0019 \tag{4}$$

The detection of IMD + O and of desnitro-IMD + 2O appears to be consistent with the formation of hydroxyl radicals through reactions 1 and 3.

https://dx.doi.org/10.1021/acs.est.9b07304
Environ. Sci. Technol. 2020, 54, 3325−3333

Table 1. Formation of NO_x after 2 h of Irradiation of IMD (10^{-4} M) or NO_3^-/NO_2^- Mixtures in Device 1

conditions	quantity of IMD converted	quantity of NO_2 formed (molar yield)	quantity of NO formed (molar yield)
IMD (10^{-4} M)	380 ± 20 μg	24 ± 5 μg (40 ± 8%)	0.88 ± 0.20 μg (2 ± 0.5%)
NO_3^- (1.8×10^{-6} M) + NO_2^- (1.7×10^{-6} M)		1.6 ± 0.3 μg	3.9 ± 0.8 μg
NO_3^- (2×10^{-5} M) + NO_2^- (5×10^{-6} M)		4.8 ± 1.0 μg	11.6 ± 2.3 μg

NO_x Formation upon Irradiation of IMD. We also measured the NO_x formation in the gaseous phase above the solutions. NO and NO_2 were successfully detected upon irradiation of IMD (10^{-4} M) in device 1. Examples of collected data are shown in Figure S2. During the first 2 h of reaction of irradiation, 24 μg of NO_2 and 0.88 μg of NO were produced, whereas the IMD loss was around 380 μg (see Table 1). After integrating the nitrite and nitrate levels produced and considering the volume of gas (200 mL) and of water (450 mL), an overall mass balance of IMD conversion into inorganic *N*-containing products was determined: 40 ± 8% for NO_2, 2 ± 0.5% for NO, 52 ± 5% for nitrate, and 16 ± 2% for nitrite.

As the presence of NO_3^-/NO_2^- in the aqueous solution could potentially generate NO_x,[33] we irradiated these ions independently to estimate their contribution to the pool of NO_x detected upon irradiation of IMD. We chose to perform these comparative experiments with NO_3^- = 1.8×10^{-6} M and NO_2^- = 1.7×10^{-6} M corresponding to the concentrations estimated after 2 h of irradiation in device 1 (Figure S4). The irradiation of this mixture for 2 h yielded 15-fold less NO_2 and 4.4-fold more NO than the irradiation of IMD (10^{-4} M) (Table 1). The amount of NO_x formed above the IMD solution was 4.5-fold higher than that above the NO_3^-/NO_2^- solution, showing that IMD was the main contributor. Moreover, the higher yield of NO in the latter system confirmed that the NO_x precursor in the NO_3^-/NO_2^- mixture was NO_2^-, through reaction 3. At higher concentrations of NO_3^-/NO_2^- (2.0×10^{-5} M and 5×10^{-6} M, respectively), not far from those reached after 16 h of IMD irradiation, NO and NO_2 levels were 3-fold higher than in the previous case, respectively, showing that, in this concentration range, the NO and NO_2 amounts accumulated in proportion to NO_2^- concentration. Again, the amount of NO_x generated from NO_2^- (2.0×10^{-5} M) was still below the one formed upon irradiation of IMD solution.

As previously shown, the bond N−NO_2 was cleaved when IMD was irradiated in the solid phase at 305 and 254 nm.[17] However, some questions remain unanswered: would the proposed mechanism in the solid phase and at short wavelengths be still valid in solution and at longer wavelengths, and thus at lower excitation energies? How is NO formed and how the oxygen atom is eliminated? In an attempt to answer these questions, we performed quantum calculations.

Theoretical Calculations. Several conformers were found for the solvated imidacloprid system. The structure of the global minimum was similar to that found from the recent first-principles[17,34] and crystallographic investigations[34] (see the Supporting Information section for all structures reported in this work). Moreover, the DFT method used here was able to reproduce accurately the experimental absorption spectrum (see Figure 3).

A detailed investigation of the ground state (S_0), the first triplet state (T_1), and the first singlet excited state (S_1) was performed. Some of the key results are shown in Figure 4 and discussed below. The minima and transition state structures are given in the Supporting Information section. The

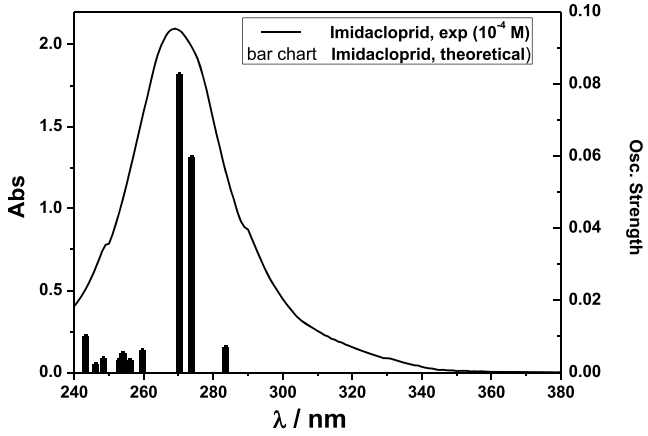

Figure 3. Experimental (Abs, left axis) and theoretical (oscillator strengths, right axis) absorption spectra of imidacloprid (theoretical spectrum for the most stable conformer (Figure S5a)) at the TD-MN12SX/6-311++G(d,p),PCM//MN12SX/6-31+G(d,p),PCM level. The oscillator strength is the probability of absorption. It is related to the dipole strength of the transition and is proportional to the molar absorptivity maximum for this transition. The S_1-S_0 transition is optically active (284 nm). The oscillator strength of this transition is 0.02, which is significant (an ε of about 6000 L·mol^{-1}·cm^{-1} can be estimated from this value, when a UV-vis half-width at half-height of 0.333 eV is used to model the absorption spectrum).

dissociation pathways of interest are depicted in this figure: NO_2 is shown on the left-hand side of Figure 4, and triplet atomic oxygen (a reaction that is precursor to the production of NO) is shown on the right-hand side of Figure 4. The minimum energy path was followed to investigate the formation of NO_2 in S_1 by performing partial optimizations of imidacloprid for fixed RN−NO_2 bond distances. The MEP maximum is indicated by a dashed level in Figure 4.

S_0 and S_1 States. Our results show that the departure of atomic triplet oxygen is not favored in the ground state because the predissociated intermediate ^{1}**RNNO−O** (R(O−O) = 1.523 Å; 56.4 kcal·mol^{-1}) cannot be reached because of very large activation energy (106.1 kcal·mol^{-1}). Similarly, the formation of NO_2 is not expected in the ground state because the respective electronic dissociation energy in S_0 is large (64.4 kcal·mol^{-1}; **RN + NO_2**). A transition state could not be found between imidacloprid (^{1}**RNNO$_2$**) and separated radicals in S_0. This is expected for homolytic dissociations in the ground state. In S_1, the dissociation of the RN−NO_2 bond required 14.0 kcal·mol^{-1} (MEP maximum). In addition, the in-cage dissociation complex ^{1}**RN···NO$_2$** is less stable (85.3 kcal·mol^{-1}) than the respective reactant (79.3 kcal·mol^{-1}). Thus, dissociation in S_1 is less favored than that in the triplet state (an activation energy of 6.1 kcal·mol^{-1} was found in T_1, and the reaction is now exothermic; see Figure 4). Moreover, our results show that the heterolytic dissociation mechanism would lead to **RN^+/NO_2^-** species, which are slightly less stable (see also Supporting Information) than the respective separated radicals (**RN/NO_2**). Thus, it seems reasonable to consider that

https://dx.doi.org/10.1021/acs.est.9b07304
Environ. Sci. Technol. 2020, 54, 3325−3333

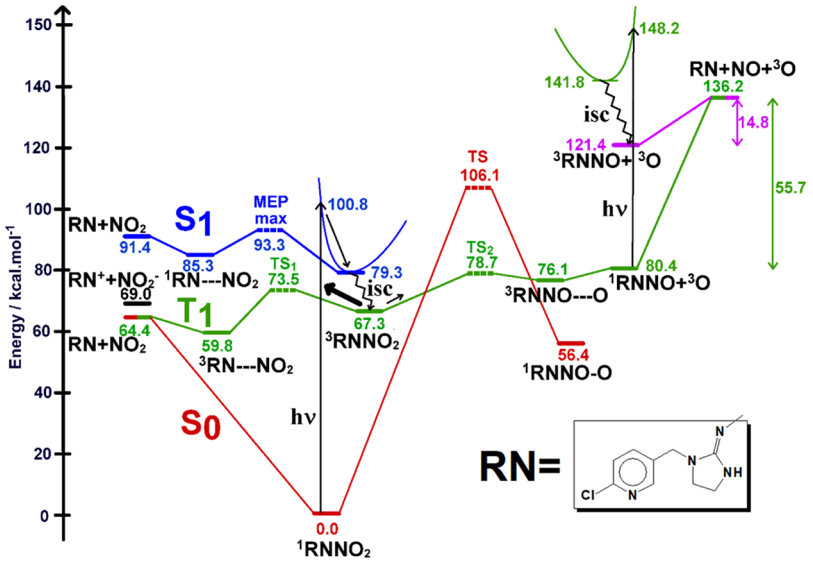

Figure 4. Electronic energies of stationary points in the ground state (S_0, red), first triplet (T_1, green), and first singlet (S_1, blue) excited states of imidacloprid (^{1}**RNNO$_2$**). Calculations were performed by the MN12SX/6-311++G(d,p),PCM//MN12SX/6-31+G(d,p),PCM method. Transition states and the MEP maximum are represented by dashed levels. Dashed bonds represent long-range separations. The energies of separated fragments **RN** + **NO$_2$** and ^{1}**RNNO** + ^{3}**O** are also given in the figure. The energies of the heterolytic dissociation products (left-hand side, black) and the triplet state of **RNNO** (right-hand side, purple) are also indicated. The separated fragments **RN** and **NO$_2$** in S_1 are, respectively, in the first doublet excited state (**RN**) and the doublet ground state (**NO$_2$**).

it is these radicals that are eventually obtained in the liquid phase. However, considering the small energy difference between heterolytic and homolytic dissociation energies, a mixture of homolytic and heterolytic dissociation products might not be completely ruled out. Implicit solvation models underestimate the solvation free energy of small ions, the cases of the proton and hydroxide being emblematic of this issue. In order to address this point, we computed $\Delta G^{*m}_{r,calc}$ the dissociation Gibbs free energy for both heterolytic and homolytic NO_2 cleavage. In this calculation, $RT \times \ln(24.46)$ was added to $\Delta G^{*}_{r,calc}$ to account for the free energy change of 1 mol of an ideal gas from 1 atm to 1 M.[35] $\Delta G^{0}_{r,calc} = \Delta G^{*}_{r,calc} + RT \times \ln(24.46)$ was 58.6 and 49.2 kcal·mol^{-1}, respectively, for the heterolytic and homolytic dissociation reactions, thus a difference of 9.4 kcal·mol^{-1} (recall that the respective difference in electronic energies was smaller, i.e., 4.6 kcal·mol^{-1}). Considering the implicit solvation model may underestimate the solvation free energy for NO_2^- by as much as 10 kcal·mol^{-1}, the radical dissociated species are still more stable than the heterolytic dissociation fragments, in agreement with our results.

Triplet State T_1. Second, S_1/T_1 intersystem-crossing (isc) is favored because minimum energy geometries in S_1 and T_1 are very similar for **RNNO$_2$**, and the energy gap is small (less than 0.1 kcal·mol^{-1} at the Franck−Condon geometry). In addition, in the triplet state, the barrier for **NO$_2$** dissociation (6.1 kcal·mol^{-1}) is significantly smaller than that for dissociation into a triplet atomic oxygen and a singlet fragment (^{1}**RNNO** + ^{3}**O**; 11.4 kcal·mol^{-1}), in agreement with our experimental findings. Moreover, the in-cage dissociation complex ^{3}**RNNO···O** is thermodynamically less stable than the respective reactant ^{3}**RNNO$_2$**, and this reaction is displaced toward the reactant. Nevertheless, this pathway is investigated below to see if this reaction could play a role, even minor, in the formation of NO radicals.

NO Formation, A Minor Pathway. The mechanism of production of nitric oxide from ^{1}**RNNO** is also shown in Figure 4. NO bond dissociation energy was 55.7 kcal·mol^{-1} for ^{1}**RNNO** in the ground state, whereas cleavage in the triplet state (reached through S_1 followed by isc) required only 14.8 kcal·mol^{-1} (**RN** is obtained). A transition state could not be found in T_1, and the energy of activation may be identified with the dissociation energy in that case. Thus, the formation of NO as a primary product from RNNO is probably a minor pathway.

Thus, our quantum calculations provide strong evidence that photolysis of IMD mainly leads to NO_2 formation in the overall triplet state's PES, while NO formation is a minor pathway.

Evidence for Nitro-/Nitroso-Derivative Formation. Nitrate and nitrite ions which generate HO$^\bullet$ radicals simultaneously with NO or NO_2 have been reported to photoinduce the nitration and/or the nitrosation of phenolic derivatives.[20−24] Whether the photolysis of IMD could also contribute to the formation of such toxic products was a hypothesis that we aimed to verify in this study. Thus, IMD was irradiated with each of the three probes, shown in Scheme 2, in a small reactor (device 2) for 16 h. Under these conditions, the loss of IMD irradiated alone reached 60% (Figure S7). We first compared the probes' consumption (10^{-4} M) in the absence and in the presence of IMD (10^{-4} M) to quantify the photoinductive effect (Table S4). The disappearance of phenol and resorcinol was drastically faster in the presence of IMD, evidencing a strong effect. Only in the case

Scheme 2. Selected Probes

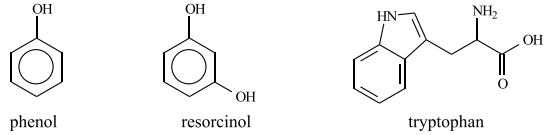

https://dx.doi.org/10.1021/acs.est.9b07304
Environ. Sci. Technol. 2020, 54, 3325−3333

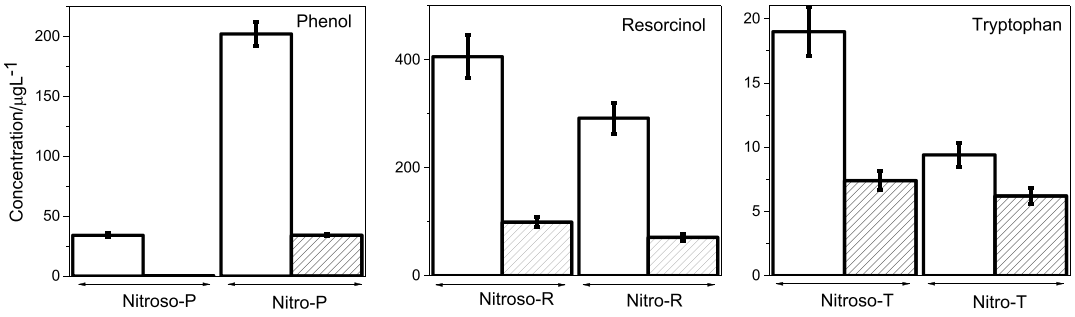

Figure 5. Concentrations of nitro- and nitroso-derivatives of phenol, resorcinol, and tryptophan detected after 16 h of irradiation of the probes (10^{-4} M) in device 2 in the presence of IMD (10^{-4} M) (white bars) and in the presence of the mixture of NO_3^- (2×10^{-5} M) and NO_2^- (5×10^{-6} M) (shaded bars). Error bars are standard deviations.

Table 2. Effect of NOM (11 mg·L^{-1}) on the Photo-Nitration/Photo-Nitrosation of Resorcinol (10^{-4} M) after 2 h of Irradiation in Device 2 in the Presence of IMD (10^{-4} M) or NO_2^- (5×10^{-6} M)[a]

conditions	% resorcinol converted	nitroso-derivatives formed (μg·L^{-1})	nitro-derivatives formed (μg·L^{-1})
IMD + resorcinol	7.0 ± 0.3	83 ± 8	44 ± 4
IMD + resorcinol + NOM	18 ± 1	110 ± 10	88 ± 9
NO_2^- + resorcinol	<1	20 ± 2	1 ± 0.1
NO_2^- + resorcinol + NOM	<1	55 ± 5	35 ± 3

[a]The light screening effect of NOM (10%) is taken into account.

of tryptophan, the acceleration effect was small because of the fast photolysis of the probe under the studied conditions.

Then, we monitored the formation of nitro-/nitroso-derivatives by UHPLC−HRMS analyses. Figure S8 shows the formation profile of nitroso- and nitro-resorcinols upon irradiation of IMD (10^{-4} M) and resorcinol (10^{-4} M). The concentration of the two photoproducts increased linearly up to 7 h of irradiation before reaching a plateau value after 16 h. Nitro- and nitroso-derivatives were also detected with phenol and tryptophan. The detected levels after 16 h of irradiation are given in Figure 5 (white bars) and Table S4. The estimated yields of nitro-resorcinols reached 3.3% of converted IMD and those of nitroso-resorcinols 5.1%. The yield of nitro-phenols (ortho + para derivatives)[21] was equal to 2.6%, but that of nitroso-phenols (ortho + para derivatives) was smaller (0.5%). For tryptophan, both yields were very small, reaching only 0.08% (nitro-derivatives) and 0.14% (nitroso-derivatives) of tryptophan converted because of the fast-direct photolysis of tryptophan.

Experiments were also performed at lower reactant concentrations to determine the impact of this parameter on the rates. A 10-fold decrease of the concentration of IMD for a concentration of resorcinol kept constant at 10^{-4} M reduced the amount of nitro-resorcinols by 18-fold and that of nitroso-resorcinols by 9-fold, while the sum of the two photoproducts was reduced by about 10-fold (Table S4). A 10-fold decrease of the concentration of resorcinol for a concentration of IMD kept constant at 10^{-4} M decreased 3-fold the amount of nitro-resorcinols and 100-fold that of nitroso-resorcinols, and their sum (nitro + nitroso) was reduced by about 5-fold (Table S4). These results indicate that the reaction rate was proportional to the concentrations of reactants. The decay rate of resorcinol followed a first-order kinetic with a rate constant k that can be expressed as: $k = 5.9 \times 10^{-3}$ [IMD] s^{-1}.

We also studied the nitro/nitrosation capacity of the NO_3^-/NO_2^- mixture to quantify their contributions in these reactions (shaded bars in Figure 5 and Table S4). For these comparisons, we fixed NO_3^-/NO_2^- concentrations to those measured in the IMD solution after 16 h of irradiation in device 2 (2×10^{-5} and 5×10^{-6} M, respectively), and the mixtures of NO_3^-/NO_2^- and probes were irradiated for 16 h in device 2. Nitrosation was 121-fold lower in the case of phenol, 4.1-fold in the case of resorcinol, and 2.6-fold in the case of tryptophan than in the presence of IMD, while nitration was 5.9-fold lower for phenol, 4.1-fold for resorcinol, and 1.5-fold for tryptophan. One concludes that the contributions of NO_3^-/NO_2^- to the nitration/nitrosation processes observed in irradiated IMD solutions were minor, especially for phenol and resorcinol, even though we acknowledge that the conditions chosen for the comparative experiments (fixed NO_3^-/NO_2^- concentrations) cannot perfectly reproduce the dynamic and complex evolution of NO_3^-/NO_2^- during IMD irradiation.

Effect of NOM on Nitration/Nitrosation of Probes. Another important aspect we attempted to explore is the effect of NOM on these photochemical nitration/nitrosation reactions. The experimental conditions and results are reported in Table 2. NOM (11 mg·L^{-1}) increased the percentage of resorcinol loss in the presence of IMD by a factor of 2.6, after correction for the light screening effects (10%). The formation of nitroso- and nitro-resorcinols in IMD solutions was increased by a factor of 1.3 and 2.0, respectively, and the formation of nitro- and nitroso-resorcinols in NO_2^- solutions by factors of 35 and 2.8, respectively. The very low formation of nitro-resorcinols in the system NO_2^- + resorcinol was already shown.[20] These data highlight the significant effect of NOM on the nitro-/nitroso-derivative formation.

Reaction Mechanism. Many reactions are expected to take place in this complex system. The main ones are summarized below. The photolysis of IMD in water generates NO_2 in the liquid phase ($NO_{2(l)}$) together with the radical RN, as shown by the quantum calculations, and the latter mainly gives rise to desnitro-IMD (reaction 5). The radicals O(^{3}P) and RNNO are also produced, but in much lower amounts (reaction 6). The reactivity of NO_2 in water is very high. It is reported in the literature that NO_3^- and NO_2^- are generated according to reactions 7a and 7b through the intermediary

https://dx.doi.org/10.1021/acs.est.9b07304
Environ. Sci. Technol. 2020, 54, 3325−3333

dimerization of $NO_{2(l)}$.[36,37] NO_3^- and $NO_{(l)}$ can also be produced through reaction 8.[37,38] In our experiments, $N_2O_{4(g)}$ cannot be distinguished from $NO_{2(g)}$. Reaction 8 is probably the major NO formation pathway, but the photolysis of RNNO (reaction 11), of $NO_{2(g)}$ (reaction 12), and of NO_2^- (reaction 3) is the alternative pathway for NO formation. NO is stable in water and volatilizes in the gaseous phase (reaction 9).[37] It generates $NO_{2(g)}$ by reacting with oxygen (reaction 10).

In this scheme, we did not take into account the oxidation of IMD by $HO^\bullet$ formed in reaction 3 because the formation of oxidation products (IMD + O) was small. NO_2^- and NO_3^- could also be oxidized by $HO^\bullet$.[39] However, because of the high concentration of IMD compared to those of NO_2^- and NO_3^- in the first half of the reaction, IMD and its main photoproduct desnitro-IMD are expected to be the main sinks of $HO^\bullet$.

$$\text{IMD} + h\nu \rightarrow NO_{2(l)} + \text{RN} \quad (5)$$

$$\text{IMD} + h\nu \rightarrow O(^3P) + \text{RNNO} \quad (6)$$

$$2NO_{2(l)} \leftrightarrow N_2O_{4(l)} \quad (7a)$$

$$N_2O_{4(l)} + H_2O \rightarrow NO_3^- + 2H^+ + NO_2^- \quad (7b)$$

$$3NO_{2(l)} + H_2O \leftrightarrow 2NO_3^- + 2H^+ + NO_{(l)} \quad (8)$$

$$NO_{(l)} \leftrightarrow NO_{(g)} \quad (9)$$

$$2NO_{(g)} + O_2 \rightarrow 2NO_{2(g)} \quad (10)$$

$$\text{RNNO} + h\nu \rightarrow NO_{(l)} + \text{radical} \quad (11)$$

$$NO_{2(g)} + h\nu \rightarrow NO_{(g)} + O(^3P) \quad (12)$$

The nitration/nitrosation of phenolic/aromatic compounds in the presence of NO_2^- or NO_3^- has already been studied.[20−25,39−41] NO_2 is recognized as having a key role in these reactions, even though the mechanisms are not fully understood. Several studies attributed the formation of phenoxyl radicals to the reaction of phenols with NO_2,[20,25,39,41] while others to their reaction with $HO^\bullet$.[40] Once formed, the phenoxyl radicals further react with NO_2 to yield the ortho- and para-derivatives of nitro-phenols. Similarly, the reaction of phenoxyl radicals with NO is expected to generate nitroso-phenols. The effect of NOM on these reactions is difficult to predict because of the existence of opposite reactions. Indeed, on the first hand, NOM can potentially favor the nitro/nitrosation reactions by generating photooxidants, such as the triplet excited states (^{3}NOM*), singlet oxygen, or $HO^\bullet$, that are expected to induce the formation of phenoxyl radicals, as shown in the literature.[39] In addition, ^{3}NOM* or $HO^\bullet$ could be able to oxidize NO_2^- and NO_3^- into NO_x[39] (see process 13 related to NO_2^-)

$$NO_2^- + {}^3\text{NOM}^*/HO^\bullet \rightarrow NO_2 + \text{NOM}^{\bullet-}/OH^- \quad (13)$$

On the other hand, NOM could also be a sink for NO_x because of the presence of aromatic moieties in its structure and therefore could inhibit the nitration/nitrosation reaction to some extent.[26,42] The overall effect of NOM will thus depend on the experimental conditions, and in particular on the relative concentrations of reactants. In our set-up, the presence of NOM (11 mg·L^{-1}) in IMD or NO_2^- solutions containing resorcinol (10^{-4} M) increased the amounts of nitro- and nitroso-resorcinols, showing that in this case, NOM favors the formation of the phenoxyl radical and of NO_2. Because Suwannee River NOM contains 68% of fulvic acids and fulvic acids contain ∼3 mmol oxidizable phenol per g of carbon,[43] there are about 20 μM of oxidizable phenols originating from NOM in a solution containing 11 mg/L. Under these conditions, where the quenching molecule is in large excess over phenolic moieties in NOM, it can be expected that the majority of NOM-derived photooxidants will be quenched by the probe compounds to form phenoxyl radicals, which can then further react with NO_x to produce nitro-/nitroso-phenol/resorcinol, enhancing the yields of these products as it is observed.

Environmental Significance. Our study showed that NO_x (NO and NO_2) could be generated by irradiation of IMD, and that these NO_x were capable of reacting with phenolic probes to produce nitro- and nitroso-derivatives. This suggests that in surface water, IMD could induce the formation of nitro and nitroso derivatives of other contaminants that could be toxicants in the aquatic environment. The importance of the phenomenon will depend on the level of IMD present in surface waters. The frequency of IMD detection in surface waters is high, and the concentration of IMD varies in a large range reaching 1 μg·L^{-1} in agricultural areas.[3,4] Based on this work and on the light absorption capacities of IMD and NO_2^-, one can calculate that at 1 μg·L^{-1}, IMD could generate as much as nitroso-/nitro-derivatives as NO_2^- at 0.1 μg·L^{-1}. The relative contributions of NO_2^- and IMD to nitroso-/nitro-derivative formation depend therefore on their levels in water. NO_2^- is present in surface waters at a maximal concentration of 0.1 mg·L^{-1}.[44] In many cases, the NO_2^- concentration will be high enough to make negligible the contribution of IMD in nitro/nitrosation reactions. However, in waters containing very low levels of NO_2^- and high levels of IMD, IMD might play a role in the nitro/nitrosation reactions.

On the other hand, we observed that NOM (11 mg·L^{-1}) enhanced the nitro and nitrosation reactions of phenols (10^{-4} M). The yield of nitro-resorcinol was multiplied by 2, whereas that of nitroso-resorcinol by 1.3, and when NO_2^- was used instead of IMD, the yields of nitro-resorcinol and of nitroso-resorcinol were increased by 35-fold and 2.8-fold, respectively. This can be explained by the enhanced formation of phenoxyl radicals in the quenching of NOM deriving photooxidants by phenols. However, this effect might be concentration-dependent. The level of NOM used in this study falls in the range of typical NOM levels found in rivers and eutrophic lakes,[45] but those of probes are high. At environmentally relevant concentrations of the probe compounds (<1 μM), phenolic moieties in NOM are in excess, and it might be possible that the NOM-bound phenoxyl radicals, at higher concentrations than the probe-derived phenoxyl radicals, might outcompete the latter for reaction with NO_x. In other words, under environmentally relevant conditions, a shift toward nitration/nitrosation of NOM seems possible, and the yield of nitro-/nitroso-derivatives of probes could then be lower compared to the ones in the absence of NOM. The incorporation of N inorganic nitrogen (N) into NOM via photolysis of nitrate/nitrite and/or in advanced oxidation process treatments was already reported and were also shown to generate potentially toxic compounds.[26−28] Therefore, such reactions might also have environmentally negative consequences. We could not detect any significant structural changes in NOM using HRMS analyses. Nevertheless, further experiments using N-labeled

https://dx.doi.org/10.1021/acs.est.9b07304
Environ. Sci. Technol. 2020, 54, 3325−3333

IMD or nitrite/nitrate and other hyphenated techniques may provide evidence for NOM nitration/nitrosation. Therefore, consistent monitoring of nitro/nitroso byproducts is highly recommended to verify their potential formation.

Our study confirms the capacity of water contaminants to interact with each other under irradiation and to induce mutual degradation. Mutual effects can involve reactions between excited- and ground-state contaminants or the intermediary formation of reactive species like NO_x in the case of IMD. Up to now, they have been poorly investigated in photochemical studies and would deserve more attention. Thus, future studies should further consider the investigation of the "cocktail effect" on the environmental fate of contaminants and more specifically the reactivity of intermediates in order to enable a more reliable monitoring of nontarget pollutants and assessment of potential risks.

■ ASSOCIATED CONTENT

Supporting Information

The Supporting Information is available free of charge at https://pubs.acs.org/doi/10.1021/acs.est.9b07304.

Spectrum of light received by the solutions in devices 1 and 2, NO_x formation in device 1 upon photolysis of IMD (10^{-4} M), calibration curve for nitroso-phenol and nitro-phenol, profiles of NO_x, NO_3^-, NO_2^-, nitroso-resorcinol, and nitro-resorcinol formation and of IMD consumption, structure and Cartesian coordinates of the minimum energy structures of IMD in S_0 (a), S_1 (b), and T_1 (c), of TS (d), of intermediate RNNO−O (e) in S_0, of TS_1 in T_1 (f), of TS_2 in T_1 (g), of ^{3}RN−NO_2 (h) and ^{3}RN−NO_2 in T_1 (i), of ^{1}RNNO (j) and ^{3}RNNO (k) at the B3LYP/6-311++G(d,p)//B3LYP/6-31+G-(d,p) level, minima and transition state structures with Cartesian coordinates, photo-nitration and photo-nitrosation of the probes after 16 h of irradiation in the presence of IMD (10^{-5} or 10^{-4} M) or a mixture of NO_3^- (2×10^{-5} M) and NO_2^- (5×10^{-6} M), and the effect of NOM (11 mg L^{-1}) on the photo-nitration/photo-nitrosation of resorcinol (10^{-4} M) after 2 h of irradiation in device 2 in the presence of IMD (10^{-4} M) or NO_2^- (5×10^{-6} M) (PDF)

■ AUTHOR INFORMATION

Corresponding Authors

Mohamad Sleiman − *Université Clermont Auvergne, CNRS, SIGMA Clermont, Institut de Chimie de Clermont-Ferrand F-63000 Clermont-Ferrand, France;* orcid.org/0000-0002-2273-1053; Email: Mohamad.sleiman@sigma-clermont.fr

Claire Richard − *Université Clermont Auvergne, CNRS, SIGMA Clermont, Institut de Chimie de Clermont-Ferrand F-63000 Clermont-Ferrand, France;* orcid.org/0000-0001-6520-5494; Phone: +33 (0)4 73 40 71 42; Email: Claire.richard@uca.fr; Fax: +33 (0)4 73 40 77 00

Authors

Davide Palma − *Université Clermont Auvergne, CNRS, SIGMA Clermont, Institut de Chimie de Clermont-Ferrand F-63000 Clermont-Ferrand, France*

Yara Arbid − *Université Clermont Auvergne, CNRS, SIGMA Clermont, Institut de Chimie de Clermont-Ferrand F-63000 Clermont-Ferrand, France*

Pascal de Sainte-Claire − *Université Clermont Auvergne, CNRS, SIGMA Clermont, Institut de Chimie de Clermont-Ferrand F-63000 Clermont-Ferrand, France*

Complete contact information is available at: https://pubs.acs.org/10.1021/acs.est.9b07304

Notes

The authors declare no competing financial interest.

The paper reflects only the author's view, and the Agency is not responsible for any use that may be made from the information it contains.

■ ACKNOWLEDGMENTS

This paper is part of a project that received funding from the European Union's Horizon 2020 research and innovation programme under the Marie Skłodowska-Curie grant agreement no. 765860 (Aquality). The authors also thank the European Regional Development Fund of the European Union and the Région Auvergne-Rhône-Alpes for financial support under the Program "Nouveau Chercheur" (no. AV0004494), which allowed the acquisition of the NO_x analyzer. We thank Martin Leremboure and Guillaume Voyard (CNRS engineers), for assistance with chromatographic and mass spectrometry analyses, and the anonymous reviewers who helped to improve the manuscript.

■ REFERENCES

(1) Jeschke, P.; Nauen, R.; Schindler, M.; Elbert, A. Overview of the status and global strategy for neonicotinoids. *J. Agric. Food Chem.* **2011**, *59*, 2897−2908.

(2) Désert, M.; Ravier, S.; Gille, G.; Quinapallo, A.; Armengaud, A.; Pochet, G.; Savelli, J.-L.; Wortham, H.; Quivet, E. Spatial and temporal distribution of current-use pesticides in ambient air of Provence-Alpes-Côte-d'Azur Region and Corsica, France. *Atmos. Environ.* **2018**, *192*, 241−256.

(3) Struger, J.; Grabuski, J.; Cagampan, S.; Sverko, E.; Mcgoldrick, D.; Marvin, C. H. Factors influencing the occurrence and distribution of neonicotinoid insecticides in surface waters of southern Ontario, Canada. *Chemosphere* **2017**, *169*, 516−523.

(4) Hladik, M. L.; Kolpin, D. W.; Kuivila, K. M. Widespread occurrence of neonicotinoid insecticides in streams in a high corn and soybean producing region, USA. *Environ. Pollut.* **2014**, *193*, 189−196.

(5) Abou-Donia, M. B.; Goldstein, L. B.; Bullman, S.; Tu, T.; Khan, W. A.; Dechkovskaia, A. M.; Abdel-Rahman, A. A. Imidacloprid induces neurobehavioral deficits and increases expression of glial fibrillary acidic protein in the motor cortex and hippocampus in offspring rats following in utero exposure. *J. Toxicol. Environ. Health. A* **2008**, *71*, 119−130.

(6) Laycock, I.; Lenthall, K. M.; Barratt, A. T.; Cresswell, J. E. Effects of imidacloprid, a neonicotinoid pesticide, on reproduction in worker bumble bees (Bombus terrestris). *Ecotoxicology* **2012**, *21*, 1937−1945.

(7) Woodcock, B. A.; Isaac, N. J. B.; Bullock, J. M.; Roy, D. B.; Garthwaite, D. G.; Crowe, A.; Pywell, R. F. Impacts of neonicotinoid use on long-term population changes in wild bees in England. *Nat. Commun.* **2016**, *7*, 12459.

(8) Berheim, E. H.; Jenks, J. A.; Lundgren, J. G.; Michel, E. S.; Grove, D.; Jensen, W. F. Effects of Neonicotinoid Insecticides on Physiology and Reproductive Characteristics of Captive Female and Fawn White-tailed Deer. *Sci. Rep.* **2019**, *9*, 1−10.

(9) Duzguner, D.; Erdogan, E. Acute oxidant and inflammatory effects of imidacloprid on the mammalian central nervous system. *Pestic. Biochem. Physiol.* **2010**, *97*, 13−18.

(10) Moza, P. N.; Hustert, K.; Feicht, E.; Kettrup, A. Photolysis of imidacloprid in aqueous solution. *Chemosphere* **1998**, *36*, 497−502.

(11) Redlich, D.; Shahin, N.; Ekici, P.; Friess, A.; Parlar, H. Kinetical study of the photoinduced degradation of imidacloprid in aquatic media. *Clean: Soil, Air, Water* **2007**, *35*, 452−458.
(12) Wamhoff, H.; Schneider, V. Photodegradation of imidacloprid. *J. Agric. Food Chem.* **1999**, *47*, 1730−1734.
(13) Zheng, W.; Liu, W. P.; Wen, Y. Z.; Lee, S.-J. Photochemistry of insecticide imidacloprid: direct and sensitized photolysis in aqueous medium. *J. Environ. Sci.* **2004**, *16*, 539−542.
(14) Schippers, N.; Schwack, W. Photochemistry of imidacloprid in model systems. *J. Agric. Food Chem.* **2008**, *56*, 8023−8029.
(15) Scholz, K.; Reinhard, F. Photolysis of imidacloprid (NTN 33893) on the leaf surface of tomato plants. *Pestic. Sci.* **1999**, *55*, 652−654.
(16) Schippers, N.; Schwack, W. Phototransformation of imidacloprid on isolated tomato fruit cuticles and on tomato fruits. *J.Photochem. Photobiol. B* **2010**, *98*, 57−60.
(17) Aregahegn, K. Z.; Shemesh, D.; Gerber, R. B.; Finlayson-Pitts, B. J. Photochemistry of thin solid films of the neonicotinoid imidacloprid on surfaces. *Environ. Sci. Technol.* **2017**, *51*, 2660−2668.
(18) Monadjemi, S.; ter Halle, A.; Richard, C. Accelerated dissipation of the herbicide cycloxydim on wax films in the presence of the fungicide chlorothalonil and under the action of solar light. *J. Agric. Food Chem.* **2014**, *62*, 4846−4851.
(19) Kouras-Hadef, S.; Hamdache, S.; de Sainte-Claire, P.; Sleiman, M.; Jaber, F.; Richard, C. Light induced degradation of the fungicide Thiophanate-methyl in water: Formation of a sensitizing photoproduct. *J.Photochem. Photobiol. A* **2018**, *360*, 262−269.
(20) Machado, F.; Boule, P. Photonitration and photonitrosation of phenolic derivatives induced in aqueous solution by excitation of nitrite and nitrate ions. *J. Photochem. Photobiol. A: Chem.* **1995**, *86*, 73−80.
(21) Vione, D.; Maurino, V.; Pelizzetti, E.; Minero, C. Phenol Photonitration and Photonitrosation upon Nitrite Photolysis in basic solution. *Int. J. Environ. Anal. Chem.* **2004**, *84*, 493−504.
(22) Suzuki, J.; Yagi, N.; Suzuki, S. Photochemical nitrosation of phenol in aqueous nitrite solution. *Chem. Pharm. Bull.* **1984**, *32*, 2803−2808.
(23) De Laurentiis, E.; Minella, M.; Berto, S.; Maurino, V.; Minero, C.; Vione, D. The fate of nitrogen upon nitrite irradiation: Formation of dissolved vs. gas-phase species. *J. Photochem. Photobiol. A: Chem.* **2015**, *307*−*308*, 30−34.
(24) Scholes, R. C.; Prasse, C.; Sedlak, D. L. The Role of Reactive Nitrogen Species in Sensitized Photolysis of Wastewater-Derived Trace Organic Contaminants. *Environ. Sci. Technol.* **2019**, *53*, 6483−6491.
(25) Vione, D.; Maurino, V.; Minero, C.; Pelizzetti, E. New processes in the environmental chemistry of nitrite: nitration of phenol upon nitrite photoinduced oxidation. *Environ. Sci. Technol.* **2002**, *36*, 669−676.
(26) Thorn, K. A.; Cox, L. G. Ultraviolet irradiation effects incorporation of nitrate and nitrite nitrogen into aquatic natural organic matter. *J. Environ. Qual.* **2012**, *41*, 865−881.
(27) Yang, P.; Ji, Y.; Lu, J.; Huang, Q. Formation of nitrophenolic byproducts during heat-activated peroxydisulfate oxidation in the presence of natural organic matter and nitrite. *Environ. Sci. Technol.* **2019**, *53*, 4255−4264.
(28) Ji, Y.; Wang, L.; Jiang, M.; Lu, J.; Ferronato, C.; Chovelon, J.-M. The role of nitrite in sulfate radical-based degradation of phenolic compounds: An unexpected nitration process relevant to groundwater remediation by in-situ chemical oxidation (ISCO). *Water Res.* **2017**, *123*, 249−257.
(29) Kieber, R. J.; Seaton, P. J. Determination of Subnanomolar Concentrations of Nitrite in Natural Waters. *Anal. Chem.* **1995**, *67*, 3261−3264.
(30) Frisch, M. J.; Trucks, G. W.; Schlegel, H. B.; Scuseria, G. E.; Robb, M. A.; Cheeseman, J. R.; Scalmani, G.; Barone, V.; Mennucci, B.; Petersson, G. A.; Nakatsuji, H.; Caricato, M.; Li, X.; Hratchian, H. P.; Izmaylov, A. F.; Bloino, J.; Zheng, G.; Sonnenberg, J. L.; Hada, M.; Ehara, M.; Toyota, K.; Fukuda, R.; Hasegawa, J.; Ishida, M.; Nakajima, T.; Honda, Y.; Kitao, O.; Nakai, H.; Vreven, T.; Montgomery, J. A., Jr.; Peralta, J. E.; Ogliaro, F.; Bearpark, M.; Heyd, J. J.; Brothers, E.; Kudin, K. N.; Staroverov, V. N.; Keith, T.; Kobayashi, R.; Normand, J.; Raghavachari, K.; Rendell, A.; Burant, J. C.; Iyengar, S. S.; Tomasi, J.; Cossi, M.; Rega, N.; Millam, J. M.; Klene, M.; Knox, J. E.; Cross, J. B.; Bakken, V.; Adamo, C.; Jaramillo, J.; Gomperts, R.; Stratmann, R. E.; Yazyev, O.; Austin, A. J.; Cammi, R.; Pomelli, C.; Ochterski, J. W.; Martin, R. L.; Morokuma, K.; Zakrzewski, V. G.; Voth, G. A.; Salvador, P.; Dannenberg, J. J.; Dapprich, S.; Daniels, A. D.; Farkas, O.; Foresman, J. B.; Ortiz, J. V.; Cioslowski, J.; Fox, D. J. *Gaussian 09*, Revision C.01; Gaussian, Inc.: Wallingford CT, 2010.
(31) Peverati, R.; Truhlar, D. G. Screened-exchange density functionals with broad accuracy for chemistry and solid-state physics. *Phys. Chem. Chem. Phys.* **2012**, *14*, 16187−16191.
(32) Vione, D.; Maurino, V.; Minero, C.; Pelizzetti, E. Reactions induced in natural waters by irradiation of nitrate and nitrite ions. *Environmental Photochemistry*; Springer-Verlag Berlin, 2005; Vol. *2*, Part M, pp 221−253.
(33) Richards-Henderson, N. K.; Anderson, C.; Anastasio, C.; Finlayson-Pitts, B. J. The effect of cations on NO_2 production from the photolysis of aqueous thin water films of nitrate salts. *Phys. Chem. Chem. Phys.* **2015**, *17*, 32211−32218.
(34) Le Questel, J.-Y.; Graton, J.; Cerón-Carrasco, J. P.; Jacquemin, D.; Planchat, A.; Thany, S. H. New insights on the molecular features and electrophysiological properties of dinotefuran, imidacloprid and acetamiprid neonicotinoid insecticides. *Bioorg. Med. Chem.* **2011**, *19*, 7623−7634.
(35) Bryantsev, V. S.; Diallo, M. S.; Goddard, W. A., III Calculation of Solvation Free Energies of Charged Solutes Using Mixed Cluster/Continuum Models. *J. Phys. Chem. B* **2008**, *112*, 9709−9719.
(36) Grätzel, M.; Henglein, A.; Lilie, J.; Beck, G. Pulsradiolytische untersuchung einiger elementarprozesse der oxydation und reduktion des nitritions. *Ber. Bunsenges. Phys. Chem.* **1969**, *73*, 646−653.
(37) Tan, S. P.; Piri, M. Modeling the Solubility of Nitrogen Dioxide in Water Using Perturbed-Chain Statistical Associating Fluid Theory. *Ind. Eng. Chem. Res.* **2013**, *52*, 16032−16043.
(38) Burdick, C. L.; Freed, E. S. The equilibrium between nitric oxide, nitrogen peroxide and aqueous solution of nitric acid. *J. Am. Chem. Soc.* **1921**, *43*, 518−530.
(39) Vione, D.; Minella, M.; Maurino, V.; Minero, C. Indirect Photochemistry in Sunlit Surface Waters: Photoinduced Production of Reactive Transient Species. *Chem.—Eur. J.* **2014**, *20*, 10590−10606.
(40) Barzaghi, P.; Herrmann, H. A mechanistic study of the oxidation of phenol by $OH/NO_2/NO_3$ in aqueous solution. *Phys. Chem. Chem. Phys.* **2002**, *4*, 3669−3675.
(41) Alfassi, Z. B.; Huie, R. E.; Neta, P. Substituent effects on rates of one-electron oxidation of phenols by the radicals ClO_2, NO_2, SO_3^-. *J. Phys. Chem.* **1986**, *90*, 4156−4158.
(42) Semitsoglou-Tsiapou, S.; Templeton, M. R.; Graham, N. J. D.; Mandal, S.; Hernández Leal, L.; Kruithof, J. C. Potential formation of mutagenicity by low pressure-UV/H2O2 during the treatment of nitrate-rich source waters. *Environ. Sci.: Wat. Res . Technol.* **2018**, *4*, 1252−1261.
(43) Ma, H.; Allen, H.; Yin, Y. Characterization of isolated fractions of dissolved organic matter from natural waters and a wastewater effluent. *Wat. Res.* **2001**, *35*, 985−996.
(44) Keeney, D.; Olson, R. A. Sources of nitrate to ground water. *Crit. Rev. Environ. Control.* **1986**, *16*, 257−304.
(45) Perdue, E. M. Natural Organic Matter. In *Biogeochemistry of Inland Waters*; Likens, G. E., Ed.; Academic Press, 2009; pp 503−516.

https://dx.doi.org/10.1021/acs.est.9b07304
Environ. Sci. Technol. 2020, 54, 3325−3333